

# Diagnosing temporal quantum correlations with compressed non-Markovian calipers

G. A. L. White,<sup>1,\*</sup> F. A. Pollock,<sup>2</sup> L. C. L. Hollenberg,<sup>1</sup> C. D. Hill,<sup>1,3,†</sup> and K. Modi<sup>2,‡</sup>

<sup>1</sup>*School of Physics, University of Melbourne, Parkville, VIC 3010, Australia*

<sup>2</sup>*School of Physics and Astronomy, Monash University, Clayton, VIC 3800, Australia*

<sup>3</sup>*School of Mathematics and Statistics, University of Melbourne, Parkville, VIC, 3010, Australia*

While the framework of non-Markovian quantum process characterisation has recently taken shape, there currently exists no practical methodology for an information-theoretic diagnostic of multitime memory effects due to hardware and scalability restrictions. Here, we present conceptual and computational methods to straightforwardly bound and benchmark any desired facet of a multitime process. We exhibit our tools on IBM Quantum computers and find surprisingly deep structures in the noisy dynamics. Namely, higher order temporal quantum correlations, including entanglement in time. Our techniques are pertinent both to generic quantum stochastic processes, and particularly to in-depth diagnostics of NISQ era quantum devices.

*Introduction.*— Achieving error rates requisite for fault-tolerant error correcting codes is a significant milestone goal in the scale-up of quantum devices. A major hurdle to this effect is the taming of correlated – either spatially or temporally – noise in quantum hardware [1–3]. The former has a robust theoretical basis, but the latter, often called non-Markovian noise, is only recently beginning to emerge as a more serious consideration [4–7]. Current measures of non-Markovianity typically offer little insight into the structure of the correlations [8–11]. In this Letter, we present an implementable strategy to capture any aspect of quantum non-Markovianity, permitting much clearer interpretations of the non-Markovian noise. These diagnostics move away from simple yes/no measures of information back-flow, and probe temporal correlations on the same footing as well-established many-body physics.

This approach is based on the foundation of process tensor tomography (PTT), which is made possible through a procedure we introduce in our adjoining Article [12] for characterisation of multi-time quantum stochastic processes. We implement these diagnostics as part of a broader theoretical result to cover hardware and scaling drawbacks of PTT. In the spirit of compressed sensing, we evaluate processes consistent with some limited dataset [13]. Importantly, the tomographically incomplete case not only reduces experimental burden, it is crucial for most current hardware that lack fast measure-and-feed-forward protocols. This departs from, for example, Ref. [5] where a primitive of non-Markovian prediction and control was possible, but a comprehensive analysis of the non-Markovianity was unattainable. Further, estimating robust non-Markovian measures scales exponentially poorly in the number of time steps. As an alternative, we introduce a family of efficient measures based on the concept of quantum Markov order [14]. These approaches each come equipped with exact bounds of desired tightness.

Specifically, we first develop a method to explore full process spaces consistent with some limited data. Consequently, we are able to find minimum and maximum

bounds on meaningful objective functions of the process in a way that resembles a caliper. These bounds may be arbitrarily tight – depending on both process purity and accessible control – and are useful for determining the strength and character of the non-Markovian noise. Next, we examine the question of ‘how much does a limited memory model fail to predict laboratory observations?’. This fine-grains previous results which typically quantify memoryless model breakdown [15, 16]. Instead, we quantify the number of previous process steps which must be accounted for to describe the dynamics up to some desired approximation. Importantly, these measures have both simple interpretations, and a clear recipe to expand the model should they fail to adequately explain the data.

While our theoretical frameworks are agnostic to the process type, we implement these methods on the IBM Quantum Experience. Our findings indicate these devices to be non-Markovian, with effects made more complex by the introduction of crosstalk, and correlations which increasingly build up over time. Remarkably, this noise is not only temporally correlated, it is naturally bipartite entangled in time, a signature of genuinely quantum non-Markovianity.

*Process tensor tomography.*— In any given experiment, there is a distinction between controllable operations implemented by the experimenter on a  $d$ -dimensional system, and uncontrollable stochastic dynamics due to system-environment ( $SE$ ) interactions. A quantum stochastic process accounts for all quantum correlations across a number of times  $\mathbf{T}_k := \{t_0, \dots, t_k\}$ . Such processes are represented as a multilinear map from a sequences of controllable operations on a system of dimension  $d$  to a final state density matrix. Here, the map, known as a process tensor [17, 18], represents all of the uncontrollable dynamics of the process. Through a generalisation of the Choi-Jamiołkowski isomorphism (CJI) [19], this mapping is encapsulated by its Choi state  $\Upsilon_{k:0}$  over  $k$  time steps as a correlated multipartite density operator. Its two-time marginals are completely positive, trace-preserving (CPTP) maps  $\hat{\mathcal{E}}_{j+1:j}$  for each se-

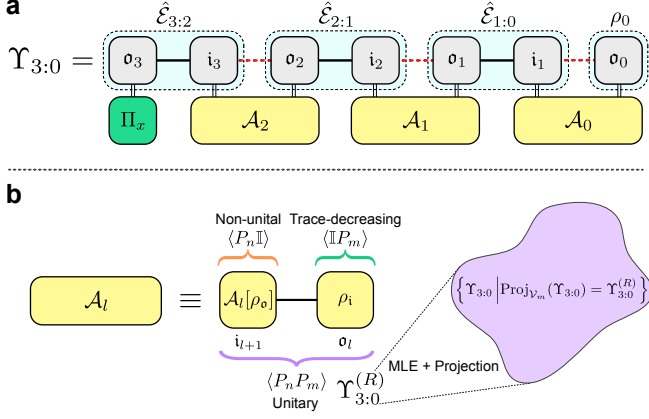


FIG. 1. **a** A 3-step process tensor Choi state. This object represents a sequence of possibly correlated CPTP maps between different points in time, plus average initial state. Output legs  $o_i$  are mapped by a control operation  $\mathcal{A}_i$  to the next input leg  $i_{i+1}$ . **b** Operation Choi states naturally partition into non-unital, trace-decreasing, and unitary controls, each as observables of  $\Upsilon_{3:0}$ . Unitary-only characterisation generates a family of process tensors consistent with the data, found through MLE.

quential pair in  $\mathbf{T}_k$ , with average initial state  $\rho_0$ . Each marginal has an input and an output tensor leg, starting from the initial state. Collectively, we label these  $\{o_k, i_k, o_{k-1}, \dots, i_1, o_0\}$  and depict the state in Figure 1a.

The operations that drive an experiment can be represented generically by a set of CP maps  $\{\mathcal{A}_0, \mathcal{A}_1, \dots, \mathcal{A}_{k-1}\}$  such that the Choi state of the full sequence is given by  $\mathbf{A}_{k-1:0} = \bigotimes_{i=0}^{k-1} \mathcal{A}_i$ . The final output, conditioned on these operations, is then given by the spatiotemporal generalisation of Born’s rule [20]:

$$\rho_k(\mathbf{A}_{k-1:0}) = \text{Tr}_{\text{in}} [\Upsilon_{k:0} (\mathbb{I}_{\text{out}} \otimes \mathbf{A}_{k-1:0}^T)]. \quad (1)$$

This generalises joint probability distributions of a classical stochastic process to the quantum regime [21]. Importantly, the description does not average over any  $SE$  dynamics or initial correlations, meaning that it naturally describes arbitrarily strong non-Markovian dynamics.

On quantum devices, this object may be reconstructed using PTT, formalised in our accompanying Article [12]. The Choi representation is fully determined by its input-output relations on an informationally complete (IC) basis of sequences of CP maps. The resulting object maps temporal correlations directly onto spatial ones, permitting standard spatial quantum information tools to be applied to the space of temporal processes. This gives rise to formal measures of non-Markovianity [22] and other properties of the dynamics, which we detail in Table I and discuss in Results sections.

*Optimising over the consistent space.*— When Equation (1) is measured experimentally for a quorum,  $\mathcal{O}(d^{4k})$ , of control sequences, the process tensor is

uniquely fixed and one can straightforwardly quantify the non-Markovian correlations [23]. Efficient unitaries, however, is typically the extent afforded to experimental control. Moreover, compressed sensing is preferable where possible. Our aim is to infer a full process and quantify non-Markovian correlation therein from given limited data. The space of  $k$ -step process tensors is given through the CJI by the set of  $2k+1$ -partite density matrices satisfying causality conditions. Specifically, they are unit-trace positive matrices satisfying  $\text{Tr}_{o_j} [\Upsilon_{j:0}] = \mathbb{I}_{i_j} \otimes \Upsilon_{j-1:0}$  for each  $j$ . Physically, causality conditions ensure that averaging over future operations does not affect the statistics of the past. Mathematically, they generate a hyperplane of dimension  $\sum_{j=1}^k (d^2 - 1)d^{4j-2}$  plus one for normalisation [12]. We denote this affine space  $\mathcal{V}_c$ .

In an accompanying Article [12], we developed a projection routine as part of maximum likelihood estimation (MLE) to impose  $\Upsilon_{k:0} \in \mathcal{S}_n^+ \cap \mathcal{V}_c$ . The main theoretical result of this Letter is to extend this in two ways here: first, we expand the affine space to include observed data, and second, we consider a range of different information-theoretic quantities as our objective to find maxima and minima. This opens up exploration of process tensor families consistent with the limited observations. The technique functions generically, however for concreteness we consider the restriction of unitary-only control sequences followed by a terminating measurement, as in Figure 1.

Consider a process tensor with decomposition  $\Upsilon_{k:0} = \Upsilon_{k:0}^{(R)} + \Upsilon_{k:0}^{(R\perp)}$ , where  $\Upsilon_{k:0}^{(R)}$  is fixed by a restricted set of experimental observations, and  $\Upsilon_{k:0}^{(R\perp)}$  its free (modulo physical constraints) orthogonal complement. In the CJI picture, unitaries are maximally entangled. Thus, there are  $d^4 - 2d^2 + 2$  nontrivial Pauli terms – the weight-2 operators and  $\langle \mathbb{I} \rangle$ . Equation (1) shows how the action of a process tensor constitutes projecting its Choi state onto the Choi state of the sequence. Correspondingly, the operation  $\mathcal{A}_l$  gives expectation values to indices  $i_{l+1}$  and  $o_l$ . The nontrivial Pauli expectations partition into non-unital  $\langle P_n \mathbb{I} \rangle$ , trace-decreasing  $\langle \mathbb{I} P_m \rangle$ , and unitary  $\langle P_n P_m \rangle$  maps, which each overlap with either marginals or correlation terms – see Figure 1b.

Now, suppose we have probed a process solely without an IC basis. Then, after treating the data with MLE, we have a set of observations  $p_{i,\bar{\mu}}$  corresponding to our restricted basis  $\mathfrak{B} := \{\mathbf{B}_{k-1:0}^{\bar{\mu}}\} := \{\bigotimes_{j=0}^{k-1} \mathbf{B}_j^{\mu_j}\}$  and POVM  $\mathcal{J} := \{\Pi_i\}$ . We can construct a new affine space  $\mathcal{V}_m$  from these observations, given by

$$\left\{ \Upsilon_{k:0} \in \mathbb{C}^{n \times n} \mid \text{Tr} \left[ \Upsilon_{k:0} \left( \Pi_i \otimes \mathbf{B}_{k-1:0}^{\bar{\mu}T} \right) \right] = p_{i,\bar{\mu}} \right\} \quad (2)$$

$$\forall \Pi_i \in \mathcal{J}, \mathbf{B}_{k-1:0}^{\bar{\mu}} \in \mathfrak{B}.$$

Consequently, the family of process tensors which are consistent with our observations is given by the intersection of the cone  $\mathcal{S}_n^+$  and the affine space  $\mathcal{V} := \mathcal{V}_c \oplus \mathcal{V}_m$

Setup	QMI (min, max)	Negativity	Purity	Fidelity	Conditional QMI*
#1. System Alone	(0.298, 0.304)	(0.0179, 0.0181)	(0.8900, 0.8904)	(0.9423, 0.9427)	(0.158, 0.178)
#2. $ +\rangle$ Nearest Neighbours (NN)	(0.363, 0.369)	(0.0255, 0.0259)	(0.7476, 0.7485)	(0.7239, 0.7244)	(0.161, 0.224)
#3. Periodic CNOTs on NNs in $ +\rangle$	(0.348, 0.358)	(0.0240, 0.0246)	(0.7796, 0.7811)	(0.7264, 0.7272)	(0.180, 0.211)
#4. $ 0\rangle$ NNs with QDD	(0.358, 0.373)	(0.0205, 0.0210)	(0.8592, 0.8612)	(0.8034, 0.8045)	(0.196, 0.221)
#5. $ +\rangle$ Long-range Neighbours	(0.329, 0.339)	(0.0209, 0.0214)	(0.8594, 0.8608)	(0.9252, 0.9260)	(0.173, 0.190)
#6. $ +\rangle$ NN, delay, $ +\rangle$ next-to-NN	(0.322, 0.329)	(0.0209, 0.0213)	(0.8534, 0.8549)	(0.9077, 0.9083)	(0.168, 0.185)

TABLE I. Property bounds on process tensors with different background dynamics. QMI measures the non-Markovianity of the process, with conditional QMI the minimal and maximal past-future dependence for first and last steps. Negativity measures unbound temporal bipartite entanglement. Purity indicates purity of the ensemble of open system trajectories, while fidelity captures the level of noise. \* Only the MLE estimate was used here, the minimum and maximum are over the space of fixed unitary operations.

(Figure 1b). As in our accompanying Article, we optimise some objective function over the feasible set using the `pgdb` algorithm [12, 24]. In short, we perform gradient descent with a chosen function, where at each iteration the object is projected onto  $\mathcal{S}_n^+ \cap \mathcal{V}$ . Akin to a caliper shifting across a region to measure, using this technique we find minimum and maximum bounds for the values that any differentiable function can take for all process tensors consistent with observed data.

*Demonstration.* – To implement this experimentally, we constructed six three-step process tensors in different dynamical setups for a system qubit on the superconducting device *ibmq\_casablanca*. These setups were designed to examine base non-Markovianity, as well as crosstalk influence. A ten-unitary basis was used, and each process tensor treated with MLE. Fixing these observations in the model, we then searched the family of consistent process tensors for a variety of diagnostic measures.

Specifically, we consider five information-theoretic quantities: **(i)** To measure total non-Markovianity, we employ quantum relative entropy,  $S(\rho||\sigma) := \text{Tr}[\rho(\log \rho - \log \sigma)]$ , between  $\Upsilon_{k:0}$  and the product of its marginals  $\bigotimes_{j=1}^k \hat{\mathcal{E}}_{j:j-1} \otimes \rho_0$ . This is a generalisation of quantum mutual information (QMI) beyond the bipartite scenario and is endowed with a clear operational meaning [22]. **(ii)** To determine whether the non-Markovianity has genuine quantum features we quantify the entanglement in the process [25, 26] by means of negativity,  $\max_{\Gamma_B} \frac{1}{2}(\|\Upsilon_{k:0}^{\Gamma_B}\|_1 - 1)$ , where  $\Gamma_B$  is the partial transpose across some bipartition [27]. **(iii)** The purity of the process,  $\text{Tr}[\Upsilon_{k:0}^2]$ , measures both the strength and size of non-Markovianity through the ensemble of non-Markovian trajectories. **(iv)** Finally, quantifying both Markovian and non-Markovian noise over multiple time steps, we compute the fidelity between the ideal process and the noisy process:  $\text{Tr}[\Upsilon_{k:0}(\bigotimes_{j=1}^k |\Phi^+\rangle\langle\Phi^+| \otimes \rho_{\text{ideal}})]$  with  $|\Phi^+\rangle = (|00\rangle + |11\rangle)/\sqrt{2}$ . Our results are summarised in Table I.

Surprisingly, we find these bounds to be extremely tight. This appears to be due to the relative purity of the process, with ranks (to numerical threshold of  $10^{-8}$ )

of between 44 and 68 for the  $128 \times 128$  matrix MLE estimates, which can limit the object’s free parameters [13]. Process rank is also directly related to the size of environment, with each nontrivial eigenvector constituting a dynamical trajectory. In practice, then, this both compresses requirements and estimates the effective dimension of the non-Markovian bath.

Interestingly, QMI is much larger than zero in all situations. Moreover, from the negativity across  $i_2$  and  $o_1$  we find temporal entanglement in all cases. Thus, not only are these noisy stochastic processes non-Markovian, they are bipartite quantum entangled in time. This includes Experiment #1, suggesting non-Markovian behaviour is prominent beyond even the immediate effects of crosstalk. Crosstalk certainly increases correlation strength, as well as decreasing process fidelity – an effect shown by switching neighbours into the  $|+\rangle$  state and coupling to  $ZZ$  noise. But  $ZZ$  noise alone cannot generate temporal entanglement [19]. We remark that when a quadratic dynamical decoupling (QDD) protocol [28] is performed on neighbouring qubits in Experiment #4, QMI increases with respect to the other experiments, but with reasonably high fidelity. This may suggest that naive QDD reduces noise strength while increasing complexity, warranting further studies.

Although this procedure is in principle to bound generic processes, in practice, we find near complete determination for only relatively few numbers of measurements. An IC three-step process tensor requires 12 288 circuits, but with only unitary gates this is 3000, so the savings are substantial. To limit experimental overhead, one might consider increasingly measuring basis sequences until bounds achieved were satisfactorily tight. This supplements, for example, machine learning approaches to directly estimate the memory [29, 30] or full characterisations [23]. With nearly unique estimates, in the final column, we also compute maximum and minimum instrument-specific memory in the form of conditional QMI (CQMI): the QMI of the Choi state when the second step is projected onto some variable unitary operation as in Figure 2a. CQMI bounds the strength of non-Markovian memory [31], which then quantifies our

ability to decouple from the non-Markovian noise. Moreover, the minimal CQMI is largest for #4, suggesting that naive decoupling may leave the noise less controllable, consistent with the observations of, e.g., Ref [32]. Nevertheless, we can leverage the size of CQMI to construct reduced memory (and complexity) models for processes.

*Rigorous model violation.*— Low CQMI in Table I indicates that conditionally finite memory processes may suffice to describe dynamics on IBM Quantum devices. In classical stochastic processes, this is known as Markov order. If marginalising over all but the previous  $\ell$  time-steps produces the same statistics for as the full joint distribution, then the process is said to have Markov order  $\ell$ . Here, this means only the previous  $\ell$  operations are relevant to the current statistics.

To efficiently estimate non-Markovianity we construct increasingly complex models, and quantify how well they describe observed device dynamics. This measure is computationally convenient, scaling linearly in time-steps; has an immediately available interpretation; and may be performed up to acceptable approximation, or where costs become prohibitive. In the quantum case, processes cannot generically exhibit Markov order. Instead, they may have a property known as *conditional Markov order* [14]. Consider three groupings of  $\mathbf{T}_k$ : past  $P$  with marginal  $\Upsilon_P$ , memory  $M$  with marginal  $\Upsilon_M$ , and future  $F$ ,  $\Upsilon_F$ . When a quantum process has conditional Markov order  $\ell$ , then for  $|M| = \ell$ , and some sequence  $\mathbf{C}_M$  acting on the memory  $\text{Tr}_M [\Upsilon_{FMP} \mathbf{C}_M^T] = \Upsilon_F^{(\mathbf{C}_M)} \otimes \Upsilon_P^{(\mathbf{C}_M)}$ , where parentheses indicate a process conditional on the choice  $\mathbf{C}_M$ . This equality is only exact for a unique IC basis, but may be approximately true for arbitrarily many control operations. The magnitude of approximation is indicated by the CQMI. In this case, only  $\Upsilon_{MP}$  and  $\Upsilon_{FM}$  are necessary. In our accompanying Article we extend the theory of quantum Markov order further by showing how overlapping memory blocks may be stitched together, and a procedure for estimating these models [12]. Conditional Markov order  $\ell$  models may be constructed by performing PTT on blocks  $M_0 := \{t_0, \dots, t_\ell\}$ ,  $M_1 := \{t_1, \dots, t_{\ell+1}\}$ ,  $\dots$ ,  $M_{k-\ell} := \{t_{k-\ell}, \dots, t_k\}$ . The estimated process tensors then collectively account for all correlations in groups of  $\ell$  sequential time steps in the object  $\Upsilon_{k:0}^\ell := \{\Upsilon_{k:k-\ell}, \Upsilon_{k-1:k-\ell-1}, \dots, \Upsilon_{\ell+1:1}, \Upsilon_{\ell:0}\}$ . Modelling a dynamical process in this manner permits studying the effects of omitting any longer time correlations [33].

We performed this procedure as an example on *ibmq-guadalupe* to observe non-Markovianity as a function of time. For a four step process, we constructed process tensors  $\Upsilon_{4:0}^\ell$  for  $\ell \in \{1, 2, 3\}$ . With a  $|+\rangle$  state neighbour, the duration of each step was varied across ten different times, ranging from 180 ns up to 1800 ns. For each value of  $t$ , we executed 100 sequences of random unitaries  $\{\mathbf{U}_{3:0}^i\}$  followed by state reconstruction. Then the action

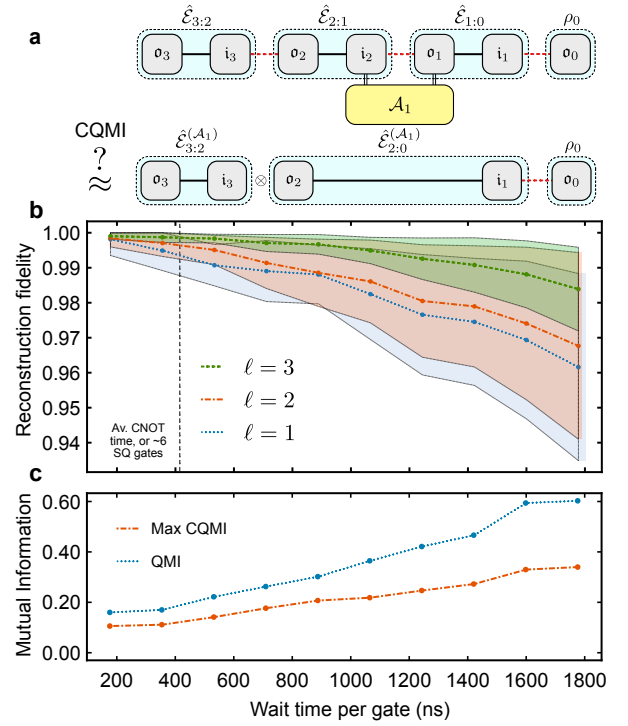


FIG. 2. Build-up of temporal correlations with increasing interaction time. **a** The CQMI quantifies the error in truncating correlations beyond  $\ell = 2$  when conditioned on intermediate operations. **b** A four step process is considered with increasing wait time after each gate. Using Markov orders  $\ell = 1$ ,  $\ell = 2$ , and  $\ell = 3$ , we quantify how each model reconstructs 100 random unitary sequences. Points indicate average fidelity, shaded regions indicate standard deviation. **c** QMI and CQMI both increase with interaction time, respectively bounding the breakdown of  $\ell = 1$  and  $\ell = 2$  models.

of  $\Upsilon_{4:0}^\ell$  on  $\mathbf{U}_{3:0}^i$  is used to predict the resulting states. The fidelity between predicted state and actual state is computed, and the distribution for each data point shown in Figure 2. We see here the build-up of memory effects; the timescales constitute relatively short-depth effective circuits, meaning these temporal correlations are likely to accumulate across practical circuits. Interestingly, the  $\ell = 3$  model performs significantly better than the other two, whereas  $\ell = 2$  is only marginally better at predicting the dynamics than  $\ell = 1$  [34]. This suggests that most of the memory effects in these devices are higher order – they persist across multiple times. Because of the cumulative build-up, for long-time dynamical processes in real situations, mitigating the effects of these correlations would require either decoupling early, or fine-graining the process into many more time steps. These memory effects manifest themselves over a time frame of only a few CNOT gates, indicating that non-Markovian dynamics are likely a significant class of noise in regular circuits.

Markovianity breakdown has been previously quantified in terms of model violation in gate sets, or in the loss

of CP divisibility [10, 35, 36]. However these approaches only coarsely diagnose temporal correlations, and are not generic to the process. We have presented a systematic framework by which different levels of finite conditional Markov order may be tested on quantum devices with both a rigorous foundation and practical interpretation.

*Conclusions.* – In this work, we have introduced a host of techniques to diagnose and quantify temporal correlations on near-term quantum processors. Since accuracy and computational requirements are at the experimenter’s discretion, these tools are also ideal for the study of natural non-Markovian quantum stochastic phenomena, where complete characterisation may be impossible [37, 38]. A future approach might be to employ statistical measures, placing confidence on the plausibility of different finite Markov models [39]. Inspecting reconstruction at the individual sequence level may also prove useful as an indication of both noise type and correlation response.

Further, we have initiated an approach to compressed descriptions of the dynamics with confidence, but it would be more desirable to have a methodical approach to determining minimal required information for a multi-time process, up to some error.

Our results on IBM Quantum devices show that non-Markovian correlations steadily build as the circuit depth increased. This prompts the need for further study of temporally correlated errors and non-Markovian behaviour on NISQ devices. This diagnostic framework can both help facilitate this, and, as indicated in Ref. [12], mitigate the effects of open systems on these devices. Understanding and addressing this complex behaviour is a necessary step on the path to fault tolerance.

*Acknowledgments.* – This work was supported by the University of Melbourne through the establishment of an IBM Quantum Network Hub at the University. G.A.L.W. is supported by an Australian Government Research Training Program Scholarship. C.D.H. is supported through a Laby Foundation grant at The University of Melbourne. K.M. is supported through Australian Research Council Future Fellowship FT160100073. K.M. and C.D.H. acknowledge the support of Australian Research Council’s Discovery Project DP210100597. K.M. and C.D.H. were recipients of the International Quantum U Tech Accelerator award by the US Air Force Research Laboratory.

---

\* [white.g@unimelb.edu.au](mailto:white.g@unimelb.edu.au)

† [cdhill@unimelb.edu.au](mailto:cdhill@unimelb.edu.au)

‡ [kavan.modi@monash.edu](mailto:kavan.modi@monash.edu)

- [1] N. H. Nickerson and B. J. Brown, *Quantum* **3**, 131 (2019), [arXiv:1712.00502](https://arxiv.org/abs/1712.00502).  
 [2] K. Rudinger, T. Proctor, D. Langharst, M. Sarovar, K. Young, and R. Blume-Kohout, *Phys. Rev. X* **9**,

- 021045 (2019).  
 [3] C. T. Chubb and S. T. Flammia, *Annales de l’Institut Henri Poincaré (D) Combinatorics, Physics and their Interactions* **8**, 269 (2021), [arXiv:1809.10704](https://arxiv.org/abs/1809.10704).  
 [4] R. Harper, S. T. Flammia, and J. J. Wallman, *Nature Physics* **16**, 1184 (2020), [arXiv:1907.13022](https://arxiv.org/abs/1907.13022).  
 [5] G. A. L. White, C. D. Hill, F. A. Pollock, L. C. L. Hollenberg, and K. Modi, *Nature Communications* **11**, 6301 (2020), [arXiv:2004.14018](https://arxiv.org/abs/2004.14018).  
 [6] B. D. Clader, C. J. Trout, J. P. Barnes, K. Schultz, G. Quiroz, and P. Titum, *Physical Review A* **103**, 052428 (2021), [arXiv:2101.11631](https://arxiv.org/abs/2101.11631).  
 [7] U. von Lüpke, F. Beaudoin, L. M. Norris, Y. Sung, R. Winik, J. Y. Qiu, M. Kjaergaard, D. Kim, J. Yoder, S. Gustavsson, L. Viola, and W. D. Oliver, *PRX Quantum* **1**, 010305 (2020).  
 [8] H. P. Breuer, E. M. Laine, J. Piilo, and B. Vacchini, *Reviews of Modern Physics* **88**, 021002 (2016).  
 [9] L. Li, M. J. Hall, and H. M. Wiseman, *Physics Reports* **759**, 1 (2018), [arXiv:1712.08879](https://arxiv.org/abs/1712.08879).  
 [10] D. Chruściński, A. Kossakowski, and A. Rivas, *Phys. Rev. A* **83**, 052128 (2011).  
 [11] S. Milz, M. S. Kim, F. A. Pollock, and K. Modi, *Physical Review Letters* **123**, 040401 (2019), [arXiv:1901.05223](https://arxiv.org/abs/1901.05223).  
 [12] G. A. L. White, F. A. Pollock, L. C. L. Hollenberg, K. Modi, and C. D. Hill, [arXiv:2106.11722](https://arxiv.org/abs/2106.11722).  
 [13] S. T. Flammia, D. Gross, Y.-K. Liu, and J. Eisert, *New Journal of Physics* **14**, 095022 (2012), [arXiv:1205.2300](https://arxiv.org/abs/1205.2300).  
 [14] P. Taranto, F. A. Pollock, S. Milz, M. Tomamichel, and K. Modi, *Physical Review Letters* **122**, 140401 (2019).  
 [15] R. Blume-Kohout, K. Rudinger, E. Nielsen, T. Proctor, and K. Young, [arxiv:2012.12231](https://arxiv.org/abs/2012.12231) (2020).  
 [16] E. Nielsen, J. K. Gamble, K. Rudinger, T. Scholten, K. Young, and R. Blume-Kohout, [arXiv:2009.07301](https://arxiv.org/abs/2009.07301) (2020).  
 [17] F. A. Pollock, C. Rodríguez-Rosario, T. Frauenheim, M. Paternostro, and K. Modi, *Physical Review A* **97**, 012127 (2018), [arXiv:1512.00589](https://arxiv.org/abs/1512.00589).  
 [18] F. Costa and S. Shrapnel, *New Journal of Physics* **18**, 063032 (2016).  
 [19] S. Milz and K. Modi, *PRX Quantum* **2**, 030201 (2021), [arXiv:2012.01894](https://arxiv.org/abs/2012.01894).  
 [20] S. Shrapnel, F. Costa, and G. Milburn, *New Journal of Physics* **20**, 053010 (2018).  
 [21] S. Milz, F. Sakuldee, F. A. Pollock, and K. Modi, *Quantum* **4**, 255 (2020), [arXiv:1712.02589](https://arxiv.org/abs/1712.02589).  
 [22] F. A. Pollock, C. Rodríguez-Rosario, T. Frauenheim, M. Paternostro, and K. Modi, *Physical Review Letters* **120**, 040405 (2018), [arXiv:1801.09811](https://arxiv.org/abs/1801.09811).  
 [23] L. Xiang, Z. Zong, Z. Zhan, Y. Fei, C. Run, Y. Wu, W. Jin, C. Xiao, Z. Jia, P. Duan, J. Wu, Y. Yin, and G. Guo, [arXiv:2105.03333](https://arxiv.org/abs/2105.03333) (2021).  
 [24] G. C. Knee, E. Bolduc, J. Leach, and E. M. Gauger, *Physical Review A* **98**, 062336 (2018), [arXiv:1803.10062](https://arxiv.org/abs/1803.10062).  
 [25] C. Giarmatzis and F. Costa, *Quantum* **5**, 440 (2021).  
 [26] S. Milz, C. Spee, Z.-P. Xu, F. A. Pollock, K. Modi, and O. Gühne, *SciPost Phys.* **10**, 141 (2021).  
 [27] Entanglement across indices  $\sigma_j$ ,  $i_j$  will trivially be large for nearly unitary processes. We care about the entanglement across indices  $i_j$ ,  $\sigma_{j-1}$ , which measures coherent quantum memory effects between time steps.  
 [28] J. R. West, B. H. Fong, and D. A. Lidar, *Phys. Rev. Lett.* **104**, 130501 (2010).  
 [29] C. Guo, K. Modi, and D. Poletti, *Physical Review A*

- 102, 062414 (2020).**
- [30] K. Goswami, C. Giarmatzi, C. Monterola, S. Shrapnel, J. Romero, and F. Costa, arXiv preprint arXiv:2102.01327 (2021).
- [31] P. Taranto, F. A. Pollock, and K. Modi, (2019), arXiv:1907.12583.
- [32] P. Jurcevic, A. Javadi-Abhari, L. S. Bishop, I. Lauer, D. F. Bogorin, M. Brink, L. Capelluto, O. Günlük, T. Itoko, N. Kanazawa, A. Kandala, *et al.*, **Quantum Science and Technology** **6**, 025020 (2021).
- [33] Y. Guo, P. Taranto, B.-H. Liu, X.-M. Hu, Y.-F. Huang, C.-F. Li, and G.-C. Guo, **Physical Review Letters** **126**, 230401 (2021).
- [34]  $\ell = 2$  and  $\ell = 1$  models can be constructed from subsets of the  $\ell = 3$  data, however on their own they minimally require  $3 \times 300 = 900$  and  $4 \times 30 = 120$  experiments per time, respectively.
- [35] R. Blume-Kohout, J. K. Gamble, E. Nielsen, K. Rudinger, J. Mizrahi, K. Fortier, and P. Maunz, **Nature Communications** **8**, 14485 (2017), arXiv:1605.07674.
- [36] G. A. L. White, C. D. Hill, and L. C. L. Hollenberg, **Physical Review Applied** **15**, 014023 (2021), arXiv:1911.12096.
- [37] N. Lambert, Y.-N. Chen, Y.-C. Cheng, C.-M. Li, G.-Y. Chen, and F. Nori, **Nature Physics** **9**, 10 (2013).
- [38] K. Sinha, P. Meystre, E. A. Goldschmidt, F. K. Fatemi, S. L. Rolston, and P. Solano, **Phys. Rev. Lett.** **124**, 043603 (2020).
- [39] S. Pethel and D. Hahs, **Physica D: Nonlinear Phenomena** **269**, 42 (2014).
- [40] D. Henrion and J. Malick, **Optimization Methods and Software** **26**, 23 (2011).
- [41] M. F. Anjos and J. B. Lasserre, **International Series in Operations Research and Management Science**, Vol. 166 (Springer US, 2012) Chap. 20, pp. XI, 960.
- [42] E. Nielsen, K. Rudinger, T. Proctor, A. Russo, K. Young, and R. Blume-Kohout, **Quantum Science and Technology** **5**, 044002 (2020).

## APPENDIX

### Choi states

The Choi representation of quantum channels used in the main text is defined as follows. The Choi-Jamiolkowski isomorphism (CJI) is the correspondence between mappings of bounded linear operators,  $\mathcal{B}(\mathcal{H}_{\text{in}}) \rightarrow \mathcal{B}(\mathcal{H}_{\text{out}})$  and bipartite quantum states on the respective spaces,  $\mathcal{B}(\mathcal{H}_{\text{out}}) \otimes \mathcal{B}(\mathcal{H}_{\text{in}})$ . Explicitly, the Choi state  $\hat{\mathcal{E}}$  of some channel  $\mathcal{E}$  on a  $d$ -dimensional system is formed by the action of  $\mathcal{E}$  on one half of an unnormalised maximally entangled state  $|\Phi^+\rangle = \sum_{i=1}^d |ii\rangle$ :

$$\hat{\mathcal{E}} := (\mathcal{E} \otimes \mathcal{I}) [|\Phi^+\rangle\langle\Phi^+|] = \sum_{i,j=1}^d \mathcal{E} [|i\rangle\langle j|] \otimes |i\rangle\langle j|, \quad (3)$$

where  $\mathcal{I}$  is the identity map. The resulting state The action of  $\mathcal{E}$  on some input state  $\rho_{\text{in}}$  is then given in terms of its Choi state by the projection

$$\mathcal{E}[\rho_{\text{in}}] = \text{Tr}_{\text{in}} \left[ (\mathbb{I}_{\text{out}} \otimes \rho_{\text{in}}^{\text{T}}) \hat{\mathcal{E}} \right]. \quad (4)$$

### Exploring process tensor families

The set of physical process tensors is convex and exists as the intersection of positive semi-definite (PSD) matrices with the affine space generated by the collection of causality conditions,  $\text{Tr}_{\sigma_j} [\Upsilon_{j:0}] = \mathbb{I}_{i_j} \otimes \Upsilon_{j-1:0} \forall j \in \{1 : k\}$ . These causality conditions may be better understood in the context of a density operator as setting expectation values of non-trivially chosen Pauli operators to zero, as outlined in our accompanying Article [12]. There, we use the pgdB algorithm to best fit experimental process tensor data. This minimises a log-likelihood cost function through gradient descent, where at each step a projection is made such that the optimisation direction is physical. We employ our own projection method which is suited to the large matrices used in process tensor analysis.

Since the causality constraints take the same form as basis measurements of the process tensor (linear inhomogeneous equations), here, we extend this method to allow for straightforward optimisation of arbitrary objective functions over the spaces of processes consistent with limited experimental data. With  $\Upsilon_{k:0} = \Upsilon_{k:0}^{(R)} + \Upsilon_{k:0}^{(R_{\perp})}$  the decomposition of a process tensor into the experimentally observed restricted process tensor,  $\Upsilon_{k:0}^{(R)}$ , and its orthogonal complement, let  $\Upsilon_{k:0}^{(R)}$  be constructed through the final-state measurement conditioned on a set of basis sequences  $\{\mathbf{B}_{k-1:0}^{\vec{\mu}}\} = \{\otimes_{i=0}^{k-1} \mathcal{B}_i^{\mu_j}\}_{\vec{\mu}=(1,1,\dots,1)}^{(d^4, d^4, \dots, d^4)}$ . Although this object has well-defined properties – such as its action on the span of its basis

elements – one cannot use it to directly estimate correlations in  $\Upsilon_{k:0}$ . For each sequence, and each measurement outcome, we have a set of equations

$$\text{Tr} \left[ \Upsilon_{k:0} \left( \Pi_i \otimes \mathbf{B}_{k-1:0}^{\vec{\mu}T} \right) \right] = p_{i,\vec{\mu}}, \quad (5)$$

which we choose to impose in our exploration of the process tensor family. To fix these, we append the expectation of each basis sequence  $\Pi_i \otimes \mathbf{B}_{k-1:0}^{\vec{\mu}}$  with its corresponding observed probability  $p_{i,\vec{\mu}}$  which describes the affine space. That is, imposing the matrix-vector equation

$$\begin{pmatrix} \langle\langle \mathcal{P}_0 | \\ \langle\langle \mathcal{P}_1 | \\ \vdots \\ \langle\langle \mathcal{P}_N | \\ \langle\langle \mathbb{I} | \\ \langle\langle \Pi_{i_0} \otimes \mathbf{B}_{k-1:0}^{\vec{\mu}_0} | \\ \langle\langle \Pi_{i_0} \otimes \mathbf{B}_{k-1:0}^{\vec{\mu}_1} | \\ \vdots \\ \langle\langle \Pi_{i_L} \otimes \mathbf{B}_{k-1:0}^{\vec{\mu}_N} | \end{pmatrix} \cdot |\Upsilon_{k:0}\rangle\rangle = \begin{pmatrix} 0 \\ 0 \\ \vdots \\ 0 \\ 1 \\ p_{i_0,\vec{\mu}_0} \\ p_{i_0,\vec{\mu}_1} \\ \vdots \\ p_{i_L,\vec{\mu}_N} \end{pmatrix}, \quad (6)$$

where  $|\cdot\rangle\rangle$  is the row-vectorisation of an operator, and  $\langle\langle \cdot |$  its complex conjugate. Each  $\mathcal{P}_i$  here is an  $n$ -qubit Pauli operator whose expectation needs to be zero for causality to follow. It is important that the observed constraints come from a procedure that guarantees the feasibility of the problem, such as a maximum likelihood estimation first. If experimental data are directly used as the set of observed probabilities, there may not exist a positive operator consistent with that data – i.e. the intersection between the affine space and PSD matrices may be empty.

Full details and benchmarking of the `pgdb` algorithm for QPT can be found in Ref. [24]. Here, we provide the pseudocode in this context, which forms the basis for our bounding of process tensor quantities.

---

#### Algorithm 1 `pgdb`

---

```

1:  $j = 0, n = d_S^{2k+1}$ 
2: Initial estimate:  $\Upsilon_{k:0}^{(0)} = \Upsilon_{k:0}^{(\text{MLE})}$ 
3: Set metaparameters:  $\alpha = 2n^2/3, \gamma = 0.3, \mu = 1 \times 10^{-3}$ 
4: while  $f(\Upsilon_{k:0}^{(j)}) - f(\Upsilon_{k:0}^{(n+1)}) > 1 \times 10^{-6}$  do
5:    $D^{(j)} = \text{Proj}_{S_n^+ \cap \mathcal{V}} \left( \Upsilon_{k:0}^{(j)} - \mu \nabla f(\Upsilon_{k:0}^{(j)}) \right) - \Upsilon_{k:0}^{(j)}$ 
6:    $\beta = 1$ 
7:   while  $f(\Upsilon_{k:0}^{(j)}) + \beta D^{(k)} > f(\Upsilon_{k:0}^{(j)}) + \gamma \beta \langle\langle D^{(j)}, \nabla f(\Upsilon_{k:0}^{(j)}) \rangle\rangle$  do
8:      $\beta = 0.5\beta$ 
9:   end while
10:   $\Upsilon_{k:0}^{(j+1)} = \Upsilon_{k:0}^{(j)} + \beta D^{(j)}$ 
11:   $j = j + 1$ 
12: end while
13: return  $\Upsilon_{k:0}^{(\text{est})} = \Upsilon_{k:0}^{(j+1)}$ 

```

---

In particular, the objective function  $f$  is chosen to be information-theoretic quantities stated in the main text (QMI, fidelity, purity, negativity), and  $\nabla f$  their analytic gradients. Extremisation of these objective functions is consequently found through projected gradient descent (or ascent), with positivity and the affine constraints (6) satisfied at each step. Algorithmic performance of the projection subroutine is contingent on the condition number of the constraint matrix. For this reason, it is important to cast the problem not necessarily in terms of the Choi states of the experimental operations, but ideally in terms of a mutually unbiased basis that spans the same space. In our case, with unitary-only control, these were the weight-2 Pauli operators on  $\mathcal{B}(\mathcal{H}_{\text{out}}) \otimes \mathcal{B}(\mathcal{H}_{\text{in}})$ . Full details of the projection subroutine

$$\text{Proj}_{S_n^+ \cap \mathcal{V}}(v_0) = \underset{v \in S_n^+ \cap \mathcal{V}}{\text{argmin}} \|v - v_0\|^2 \quad (7)$$

can be found in Refs. [12, 40, 41]. In short, let  $|\Upsilon_{k:0}\rangle\rangle := v_0$ , let  $\kappa \in \mathbb{R}^m$  for  $m$  affine constraints, and let the terms in Equation (6) be denoted  $A \cdot v = b$ . Diagonalising  $\Upsilon_{k:0}$  gives  $\Upsilon_{k:0} = UDU^\dagger$  where  $D = \text{diag}(\lambda_1, \lambda_2, \dots, \lambda_n)$  is real.

Then the projection onto  $\mathcal{S}_n^+$  is:

$$\text{Proj}_{\mathcal{S}_n^+}(\Upsilon) = U \text{diag}(\lambda_0^+, \dots, \lambda_n^+) U^\dagger \quad (8)$$

with  $\lambda_j^+ := \max\{\lambda_j, 0\}$ . Now, defining  $v(\kappa) := \text{Proj}_{\mathcal{S}_n^+}(v_0 + A^\dagger \kappa)$  (note that projection of a vector here carries implied matrix reshape, positive projection, followed by vector reshape), it can be shown that the unconstrained minimisation of the function

$$\theta(\kappa) = -\|v(\kappa)\|^2 + b^\dagger \kappa, \quad (9)$$

whose gradient is

$$\nabla \theta(\kappa) = -Av(\kappa) + b, \quad (10)$$

is the unique solution to Equation (7). For our purposes then, we employ the L-BFGS algorithm to minimise  $\theta(\kappa)$ , and thus project some  $v_0$  onto  $\mathcal{S}_n^+ \cap \mathcal{V}$ .

### Overview of experiments

Here, we discuss the details of the IBM Quantum experiments conducted in the main text. *ibmq-casablanca* is a 7-qubit and *ibmq-guadalupe* a 16-qubit superconducting transmon device with quantum volumes of 32. The layout of the former is shown in Fig 3a and the structure of the process tensor experiments in Fig 3b.  $q_5$  was used as the system qubit for all experiments shown in the main table, and had a measured  $T_2$  time of 123.65  $\mu\text{s}$  during the period over which data was collected. For experiments #1–#6 the backgrounds were varied, and the wait time between each time step identically fixed to 1.28  $\mu\text{s}$ . A ten-unitary basis was used, for a total of 3000 circuits per experiment at 4096 shots. The details of each background are as follows:

1. No control operations on any other qubits.
2.  $q_3$ ,  $q_4$ , and  $q_6$  were each initialised into a  $|+\rangle$  state at the beginning of the circuits and left idle.
3.  $q_3$ ,  $q_4$ , and  $q_6$  were each initialised into a  $|+\rangle$  state at the beginning of the circuits, and, in each wait period, four sequential CNOTs controlled by  $q_3$  and with  $q_1$  as a target were implemented.
4.  $q_3$ ,  $q_4$ , and  $q_6$  were all dynamically decoupled using the QDD scheme with an inner loop of 2  $Y$  gates and an outer loop of 2  $X$  gates. i.e. a sequence  $Y-Y-X-Y-Y-X-Y-Y$ .
5.  $q_0$ ,  $q_1$ , and  $q_2$  were initialised into a  $|+\rangle$  state and left idle.
6.  $q_3$  was initialised into a  $|+\rangle$  state, followed by a wait time of 320 ns, and then  $q_1$  also initialised into a  $|+\rangle$  state and left idle.

To account for the effects of measurement errors on the process estimates, we first performed gate set tomography (GST) on the system qubit using the `pyGSTi` package [42]. This was used to obtain a high quality estimate of the POVM  $\{|+\rangle\langle+|, |-\rangle\langle-|, |i+\rangle\langle i+|, |i-\rangle\langle i-|, |0\rangle\langle 0|, |1\rangle\langle 1|\}$ , which was then used in the maximum likelihood estimate of each process tensor.

In the conditional Markov order reconstruction, the device *ibmq-guadalupe* was used, with a circuit structure the same as Figure 3b, but with four operations and a variable duration between gates. The system qubit had a measured  $T_2$  of 128.02  $\mu\text{s}$  during the period of the experiments. At the start of each run, the neighbouring qubit to the system is initialised in the  $|+\rangle$  state and left idle. Reconstruction of the memory process tensors  $\Upsilon_{3:0}$  and  $\Upsilon_{4:1}$  is performed as in our accompanying Article [12], as well as their collective action on the set of operations. In total, for the ten time frames, this required  $2 \times 3000 \times 10 = 60\,000$  circuits for the  $\ell = 3$  case.

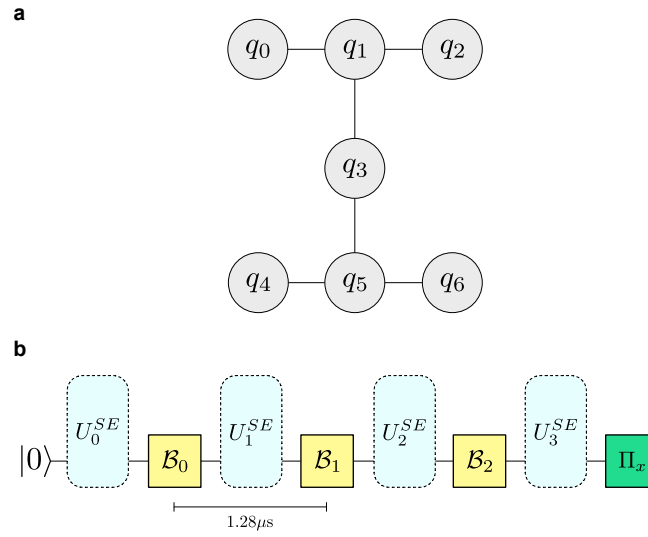


FIG. 3. **a** Qubit map of *ibmq\_casablanca*,  $q_5$  was the system qubit in all experiments. **b** Structure of the process tensor circuits for this device: a three-step process tensor constitutes three basis operations, followed by measurement. For all six experiments, we fixed the wait time at  $1.28 \mu\text{s}$  and varied the background.